Nanoscale

PROTEIN ADSORPTION INDUCED BRIDGING FLOCCULATION: THE DOMINANT ENTROPIC PATHWAY OF NANO-BIO COMPLEXATION

SCHOLARONE™
Manuscripts

1   **PROTEIN ADSORPTION INDUCED BRIDGING FLOCCULATION: THE**
2   **DOMINANT ENTROPIC PATHWAY OF NANO-BIO COMPLEXATION**

3   Necla Mine Eren[1,2,3], Ganesan Narsimhan[1,3] and Osvaldo Campanella[1,3]

4
5   [1]Agricultural and Biological Engineering, Purdue University, West Lafayette IN
6   [2]Industrial and Physical Pharmacy, Purdue University, West Lafayette IN
7   [3] Whistler Center for Carbohydrate Research, Purdue University, West Lafayette IN
8

9   **Abstract**

10   Lysozyme-silica interactions and resulting complexation were investigated through
11   adsorption isotherms, dynamic and electrophoretic light scattering, circular di-chroism (CD), and
12   isothermal titration calorimetry (ITC). A thermodynamic analysis on ITC data revealed the
13   existence of two binding modes during protein-nanoparticle complexation. Both binding modes
14   are driven by the cooperation of favorable enthalpy in the presence of a dominating entropy gain.
15   The first binding mode has a higher binding affinity, lower equilibrium stoichiometry and is
16   driven by a higher entropic contribution compared to the second type. The observed favorable
17   enthalpy gain in both modes is attributed to non-covalent complexation whereas the entropy gain
18   is associated to the re-organization of the silica surface including not only the solvent and
19   counter ion release, but also protein's conformational changes. Possible mechanisms are
20   proposed to explain non-covalent complexations for each binding mode by relating the changes
21   in the zeta potential and hydrodynamic radius to the obtained adsorption isotherms and
22   calorimetry profile. Based on all these findings, it is proposed that lysozyme adsorption on nano-
23   silica is the result of protein-nanoparticle and protein-protein interactions that further leads
24   spontaneous, non-directional and random complexation of silica through bridging flocculation.

25   **Introduction**

26   Nanoparticle-protein interactions are at the heart of today's nanotechnology research [1-7].
27   Not only they determine the biological response to nano-medical tools [8,9], but they also
28   determine the functionality of non-medical nano-applications that interface nanoparticles with
29   proteins [10]. Immobilization of enzymes, design of biosensors and nano-bio hybrid materials are
30   examples of nano-applications that are not directly related to medicine [11,12]. Among those,
31   nano-bio hybridization with proteins can be defined as a spontaneous complexation process in
32   which specific and weak interactions between proteins and nanoparticles triggers self-assembly
33   of organic and inorganic components into two-dimensional networks and three dimensional
34   structures [13,14]. The functional properties of the those networks and structures depend on the
35   nanoparticle surface characteristics [15], size [16] and shape [17] of the nanoparticles, supra-

36   chemical reactivity [18] and internal structure rigidity [19] of proteins, the physicochemical
37   characteristics of the surrounding solvent [20] and the nanoparticles/protein concentration ratio [21]
38   . Despite the fact that the wide range window of parameters offers increased functional diversity,
39   the complexation mechanisms are so broad and unspecific that the development of design
40   strategies to produce nano-bio complexes with targeted functional properties becomes difficult
41   [13,14,22] . This gap most probably stems from the lack of understanding of thermodynamical
42   principles that are involved in nano-bio complexations.

43   The current study was stimulated by a central curiosity about the thermodynamic details
44   of a "spontaneous" complexation process. In order to focus more on the mechanism of the
45   complexation, rather than system component characterization, the complexation of lysozyme
46   with hydrophilic silica was chosen as a model system.

47   The rationale behind the model system selection can be summarized as follow: 1)
48   structure, size, shape and surface characteristics of each component is well-documented [23-25] 2)
49   interactions of lysozyme with silica have been extensively studied using different approaches
50   that complement the thermodynamic approach [26-30] utilized in this work 3) both materials are
51   abundant, inexpensive and preparation of samples for experiments does not require specific
52   expertise and longtime purification procedures.

53   The specific objectives were 1) to investigate the model system interactions via
54   traditional adsorption isotherms, isothermal titration calorimetry (ITC), dynamic and
55   electrophoretic light scattering and circular di-chroism (CD), 2) to compare Langmuir and Hill
56   models in order to quantitatively assess the adsorption of the protein on the nano-particles and 3)
57   to describe the heat of binding through a complexation mechanism that accounts for both
58   enthalpic and entropic contributions.

59   The central motivation behind the specific objectives was to investigate the mechanism of
60   nano-bio complexation. It is expected that the mechanisms of interactions at the nanoparticle-
61   biopolymer (like for example proteins) interface will be better understood with other studies
62   conducted using different model systems, under different conditions and even with different or
63   similar approaches as the one presented in this work. The gain of more fundamental
64   understanding of these complexation mechanisms will lead to more specific applications that use
65   or include proteins and nanoparticles either as disordered fractal like microstructures or highly
66   ordered crystals [13, 14, 22].

67   **Experimental**

68   **Materials and methodology**

69   Silica nanoparticles (Ludox-TM50, 20 nm, Polydispersity Index=0.06) used in the study
70   were donated by Grace& Co.-Conn (MD, USA). Chicken egg white lysozyme (L6876, ellipsoid

71   dimensions=4.5x3x3 nm, Polydispersity Index=0.07) was purchased from Sigma-Aldrich (MO,
72   USA). Both protein and silica solutions/suspensions were prepared in sodium phosphate buffer
73   (10mM, pH=7.4±0.1, protein was dialyzed against buffer) at various concentrations to obtain
74   lysozyme/silica molar ratios ranging from 5 to 200. All the experiments were conducted in a
75   similar manner to the ITC method; complexation was assumed to reach equilibrium in 5 minutes
76   after each injection corresponding to the particular molar ratio. All the experiments were
77   conducted at room temperature and in triplicate.

78   **Adsorption Isotherms with depletion method**

79   In order to obtain adsorption isotherms the Norde's depletion method [30] was followed
80   with slight modifications: 1) Unbound protein concentration was determined with the BCA assay
81   according to the manufacturer's standard test tube protocol that has a detection range of 20-
82   200μg/mL (Thermo Scientific, IL,USA). 2) Silica suspensions with the same concentration were
83   titrated with protein solutions similar to the ITC technique (See the ESI, Table ESI-1).

84   **Complex Characterization with DLS, ELS and TEM**

85   Dynamic Light Scattering (DLS) was performed on a light scattering goniometer
86   (ALV/CGS-3 Compact Goniometer, ALV, Langen, Germany), and measurements were
87   conducted using 10 mm diameter glass tubes and illuminated with a HeNe laser (wavelength
88   was 632.8 nm and output power 22 mW). Scattered light was detected with dual ALV-High QE
89   APD (avalanche photo diode) photon detectors in Pseudo-Cross-Correlation Mode at an angle of
90   90° for 120 seconds. The cumulant method was used to determine the mean hydrodynamic
91   radius (Rh) of the lysozyme-silica complexes [31].

92   Electrophoretic mobility at 25 °C was determined in disposable folded capillary cells
93   (DTS1070, Malvern, Worcestershire, UK) with a zeta-sizer that combines laser Doppler
94   velocimetry and phase analysis light scattering (Zeta-sizer Nano ZS, Malvern, Worcestershire,
95   UK). Electrophoretic mobility (U_E) was converted to zeta potential (z) using Henry Equation,
96   ($U_E = 2\varepsilon z f(ka)/3\mu$)) using the Smoluchowski approximation ($f(ka) = 1.5$), where ε and μ are
97   the dielectric constant and the viscosity of the continuous phase that were assumed to be 78 and
98   0.89 cP, respectively. The scattering angle was 173° and refractive index of silica and protein
99   were assumed as 1.33 and 1.45, respectively [32]. The protein's refractive index was used for
100 silica-protein mixtures.

101 TEM images, used for the graphical abstract, were obtained through the use of copper
102 grids and a FEI/Philips CM-100 TEM instrument by negative staining with phosphotungstic acid
103 [33].

104 **Secondary structure of free and bound protein with CD**

105   CD spectrum was collected for wavelengths in the range of 260-185 nm with a Jasco J-
106   1500 CD spectrometer equipped with a temperature controller. The bandwidth was 1 nm and
107   scanning speed was 50 nm/min. Collected spectra in mdeg was converted to mean residual
108   ellipticity [34] and deconvolution was performed with the DichroWeb online server using the
109   CDSSTR algorithm and the reference data set 3 [35-36] (See the ESI, Figure 1a-c).

Heat of interactions with ITC

111   Isothermal titration calorimetry was carried out with a Nano ITC calorimeter (TA
112   Instruments, DE, USA). The reference cell was filled with water, whereas the reaction cell was
113   filled with the silica suspensions. The protein solution was injected into the reaction cell at
114   intervals of 300 sec and a stirring speed of 350 rpm until saturation (if necessary, a second
115   syringe was used for injection after the first load). All the blank experiments (heat of dilution,
116   heat of injection, heat of mixing) were conducted under the same conditions [37]. Heat profile was
117   fitted with the multiple site model to obtain the thermodynamic parameters [38].

118   **Results**

119   **Protein Adsorption**

120   Different types of adsorption isotherms were constructed by plotting the surface coverage
121   (Γ) versus equilibrium protein concentration (Ceq) (Figure 1), the adsorbed protein mass versus
122   Ceq, the surface coverage fraction (Γ/Γ_{max}) versus mole ratio (lysozyme/silica) and Ceq versus
123   mole ratio (ESI Figure 1. a-c). Figure 1 is the most traditional way to depict the characteristics
124   of polymer adsorption on solid surfaces, and under specific assumptions (summarized below in
125   the discussion section) the thermodynamic equilibrium constant of the protein surface
126   interactions could be calculated by using the Langmuir (Eqn 1) and Hill (Eqn 2) models.

$$\Gamma = \frac{\Gamma_{max} C_{eq}}{K_{app} + C_{eq}}$$

127   *(Eqn*
128   *1)*

$$\Gamma = \frac{\Gamma_{max} C_{eq}{}^{n_{hill}}}{K_{app} + C_{eq}{}^{n_{hill}}}$$

129   *(Eqn 2)*

130   Where Γ is the surface coverage (mg/m^2), Γ_{max} is the maximum surface coverage
131   (mg/m^2), C_{eq} is the equilibrium protein concentration (mg/mL), K_{app} is the apparent dissociation
132   constant (mg/mL) and (n_{hill}) is the cooperativity term.

133   By fitting the experimental data with the Langmuir and Hill models the maximum surface
134   coverage Γ_{max} was calculated as 1.51 mg/m^2 and 1.27 mg/m^2, respectively. Corresponding

135   apparent dissociation constants were 65×10^{-6} (Langmuir) and 3.15×10^{-8} (Hill) .It could be noted
136   that even without using any assumption or an assumed fitting model the experimental data shows
137   that the adsorption isotherm reaches a plateau around 1.3 mg/m^2 (Figure 1). This is in agreement
138   with previously reported maximum surface coverage of lysozyme on hydrophilic silica at neutral
139   pH and low ionic strength and this well-defined plateau corresponds to full coverage of the
140   surface [30]. Also the initial steep of the isotherm reflects the high binding affinity of lysozyme on
141   oppositely charged hydrophilic silica which is quite reasonable for a globular, structurally stable
142   protein [39].

143   **Protein Adsorption Induced Silica Flocculation**

144   The zeta potential (ζ) and hydrodynamic radius of lysozyme-silica complexes were
145   determined for various molar ratios to track the electrostatic interactions driving the complex
146   formation and to roughly quantify the size of formed complexes, respectively (Figures 2A and
147   2B).

148   Protein adsorption modifies the silica surface charge dramatically (initially -41 mV) even
149   at low protein loadings, followed by the charge neutralization (at a molar ratio between 18.8 and
150   23.5) and charge is reversed until the charge of the complex is equal to that of native free
151   lysozyme (10mV). Charge neutralization and reversal is a quite expected outcome of the
152   electrostatic interactions between oppositely charged surfaces [40].

153   The other consequence of lysozyme adsorption on hydrophilic silica is bridging
154   flocculation[20,41]. Even at the very low protein loading (molar ratio=4.7, ζ=-33.2 mV),
155   hydrodynamic radius of lysozyme-silica complex (469 nm) is much larger than that of silica (20
156   nm) and lysozyme (4 nm) indicating the formation of silica aggregates linked via adsorbed
157   lysozyme (Figure 2B). At higher protein loadings aggregate size exceeds 2 μm which is similar
158   to the aggregate size of silica/lysozyme flocculates that has been determined by other researchers
159   using the sedimentation velocity technique [20].

160   **Protein Denaturation upon Adsorption**

161   CD spectra of native lysozyme and silica-lysozyme mixtures at 2 different molar ratios
162   (MR): lysozyme/silica=47.2 and lysozyme/silica=94.3, were collected. Control refers to the
163   native protein in buffer without any silica (Figure 3A). It is important to note that while
164   converting the CD raw signal (millidegrees) to mean residual ellipticity (MRE), initial protein
165   concentration (bound plus free) of silica-lysozyme mixtures was used to obtain the total
166   conformational change in the whole system which is composed of bound and free protein. The
167   focus was not to isolate the CD signal of the adsorbed state or determine the surface coverage
168   dependent structural changes since those aspects have been already reported with great detail [42].

169 According to the BCA assay, at a MR =47.2, almost 90% of the total protein in the
170 system is bound to silica nanoparticles. Thus, at this molar concentration CD signal is mostly
171 coming from the bound protein since free protein concentration (Ceq=0.05) is very low for the
172 provided relatively small path length (0.01 cm). On the other hand, at MR=100, bound protein
173 accounts for the 50% of the total protein in the system which refers to the equilibrium
174 stoichiometry.

175 Perturbation of the secondary structure upon binding is clearly visible from the changes
176 in the CD spectra even without de-convolution. Otherwise, CD spectra should have overlapped
177 once plotted in MRE units. Upon adsorption, magnitudes of the negative peaks at 222 nm and
178 208 nm as well as the magnitude of the positive peak at 193nm decreased. Also, negative peak
179 shifted towards to 218 nm and positive peak shifts towards to 195 nm. This clearly indicates a
180 decrease in the alpha-helix and an increase in beta-sheet and random coil conformations, which
181 is in agreement with earlier reports examining lysozyme structural changes upon adsorption on
182 solid surfaces [30,42-46] .

183 To further understand the changes in the protein CD spectra upon adsorption on the silica
184 surface, fractions of secondary structure components were calculated by deconvolution of the
185 CD spectra. According to the deconvolution of CD spectra, native lysozyme has a conformation
186 composing 33.7 % helix, 18.7 % sheet, 22.5% turn and 25.7% unordered structures which is in
187 general agreement with the secondary structure fractions of lysozyme reported from X-Ray data
188 [47] (helix:0.39, sheet:0.11, turn:0.34 and unordered:0.16), ATR/FTIR [48] (helix:0.40, sheet:0.07,
189 turn:0.4 and unordered: 0.13) and CD in phosphate buffer [34] (helix:0.34 sheet:0.17 turn:0.23
190 unordered:0.26). To compare secondary structure components of native protein and bound
191 protein at different molar ratios, the three situations described above were plotted together
192 (Figure 3B).

193 According to the deconvolution results, the structure of lysozyme was perturbed
194 significantly upon adsorption (18% loss in helical structure, 14 % gain in sheets and 4% gain in
195 random coil conformations). The extent of the conformational changes is quite comparable with
196 earlier reports that investigated the perturbation of lysozyme on similar hydrophilic silica
197 particles at neutral pH (20-32 % loss in helical structure [42-45], 14% gain in sheets and 6% gain in
198 random coil [42].

199 **Thermal Footprints of Adsorption Induced Flocculation**

200 The thermodynamic nature of the interactions between lysozyme and silica was further
201 investigated using isothermal titration calorimetry (ITC) in order to resolve the specific
202 contributions of the driving forces that dominate the complex formation. As lysozyme is titrated
203 into the calorimeter sample cell that contains silica, the heat change in the sample cell is
204 compensated by the applied power to maintain the thermal equilibrium with the reference cell. If

205   heat is released, the sample cell would require less power input (negative signal), whereas
206   absorption of heat would require more power input (positive signal). Observed negative signal
207   through the entire range of titration reflected the overall exothermic nature of all interactions
208   among the system components: protein, nanoparticle and solvent (Figure 4A). Raw data peaks
209   were (i) integrated with respect to time, (ii) corrected for the heat of dilution, heat of injection
210   and heat of mixing, (iii) normalized with respect to molarity of titrant to obtain the molar
211   enthalpy of the interactions (Figure 4B). To further quantify the association constant (K_a),
212   enthalpy change (ΔH) and stoichiometry (n) from the heat profile, a curve-fitting analysis was
213   performed using the multiple site model. Gibbs free energy change (ΔG) and entropy change
214   (ΔS) were calculated from the following equations:

215    $$\Delta G = -RT \ln K_a \qquad\qquad\qquad\qquad\qquad\qquad\qquad (Eqn\ 3)$$

216    $$\Delta G = \Delta H - T\Delta S \qquad\qquad\qquad\qquad\qquad\qquad\qquad (Eqn\ 4)$$

217   where R is gas constant, T is the absolute temperature, K_a the equilibrium constant for
218   complexation and ΔH is the enthalpy change during the complexation.

219   Thermodynamic parameters of nanoparticle-protein interactions (K_a, n, ΔH, ΔG, ΔS)
220   obtained from the ITC experimental data are summarized in Table 1.
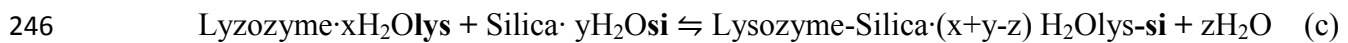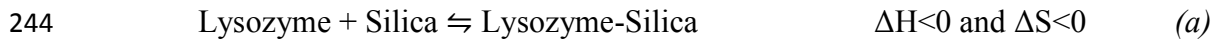
221   According to curve fitting analysis the overall complexation of nanoparticle and protein
222   features two distinct binding modes with significantly different affinities, stoichiometry's and
223   enthalpies. The first site binds with larger affinity and enthalpy whereas the second site binds
224   with weaker affinity and larger stoichiometry/population of sites resulting in a weaker enthalpy
225   per molecule. Even though both binding modes feature favorable enthalpic changes ($\Delta H<0$), and
226   entropic changes ($\Delta S>0$), the entropic contribution is less prominent in the second binding mode.

227   Observation of two discrete binding events is quite rare in published titration calorimetry
228   studies. Nevertheless, there are some influential work that successfully resolved the binding
229   curve for two binding modes [16,49,50]. In one of those studies, a detailed protein-nanoparticle
230   complexation mechanism that accounts for both non-covalent complex formation and solvent
231   reorganization was proposed [16]. The proposed De's mechanism is adapted and incorporated in
232   this work in order to draw an overall thermodynamic view explaining lysozyme interactions with
233   hydrophilic silica.

234   According to De's mechanism, the complexation of nanoparticles with proteins could be
235   exothermic or endothermic depending on the nature of interactions driving the complex
236   formation. As long as favorable enthalpy contribution ($\Delta H<0$, exothermic) is not offset by an
237   unfavorable entropy loss ($\Delta S<0$) or an unfavorable enthalpy contribution ($\Delta H>0$, endothermic) is
238   compensated by a favorable entropy gain ($\Delta S>0$), free energy of the process (ΔG) will be

239   negative. Negative free energy change is the thermodynamic requirement for a process to occur
240   spontaneously.

241   Based on those thermodynamics conditions, the overall lysozyme-silica complexation
242   process (reaction *c* below) could be described as a combination of a non-covalent complex
243   formation (reaction *a*) and a solvent reorganization reaction (reaction *b*).

244   Lysozyme + Silica $\leftrightharpoons$ Lysozyme-Silica $\Delta H<0$ and $\Delta S<0$ *(a)*

245       $xH_2Olys + yH_2Osi \leftrightharpoons (x+y-z)H_2Olys\text{-}si + zH_2O$ $\Delta H>0$ and $\Delta S>0$ *(b)*

246   Lyzozyme·xH_2Olys + Silica· $yH_2Osi \leftrightharpoons$ Lysozyme-Silica·$(x+y-z) H_2Olys\text{-}si + zH_2O$ (c)

247   where H_2Olys, H_2Osi, $H_2Olys\text{-}si$ are water molecules bound to lysozyme, silica and
248   lysozyme-silica complexes, respectively.

249   In reaction *a*, formation of non-covalent bonds are favorable and could compensate the
250   loss of conformational entropy due to complex formation [16]. In reaction *b* energy is required for
251   disruption of the bound water at the nanoparticle-protein interface ($\Delta H>0$), but the increasing
252   conformational entropy of water ($\Delta S>0$) due to the release of highly ordered solvent from
253   interface to bulk could compensate the unfavorable enthalpy contribution. So the enthalpy and
254   entropy changes in reaction *c* would be a sum of those contributions, resulting in a feasible
255   process with a negative change of Gibbs free energy. With these results it becomes clear that in
256   each binding mode the contribution of those processes weight differently. For the first binding
257   mode increase in entropy is the dominating driving force for the complexation and for the second
258   complexation mode the process is driven by a moderately favorable enthalpy and a moderately
259   favorable entropy contribution (Figure 5).

260   In addition to the entropy changes due to solvent release/reorganization, the effects of the
261   counter ion release should be also considered for all low ionic strength systems [51-53]. In this
262   study, when lysozyme comes into contact with charged silica surface, a considerable fraction of
263   mobile counter ions surrounding the protein and the inorganic surface might be releasing to the
264   bulk solution. Thus, the entropy gain associated with the increase in the counter ions'
265   translational entropy could be incorporated into the reaction *b*, along with the solvent release and
266   reorganization.

267   **<u>Discussion</u>**

268   **Non-Direct Methods to evaluate Mechanisms of Protein Adsorption**

269   When a small gas molecule approaches to a solid interface, only two things might
270   happen: adsorption on or desorption from the surface. On the other hand, when a protein
271   molecule approaches to a solid surface, protein might undergo structural arrangements, interact
272   with each other, change the surface affinity depending on the surface coverage, form multiple

273   layers all of which complicates the adsorption and desorption process. The Langmuir adsorption
274   theory and model has been developed for gases and serves only as a starting point to model the
275   complicated protein adsorption behavior [54-56]. Thus, in order to characterize the mechanistic
276   details of the protein adsorption process, high resolution real time kinetic experimental data
277   should be described by advanced mathematical models that take into account all the deviations
278   from idealized situations included in the hypotheses used to develop the Langmuir theory [55]. In
279   addition, thermodynamic models can also reveal energetic aspects of the adsorption process and
280   can be applied using final equilibrium concentrations and surface coverages to calculate
281   equilibrium constants and the associated thermodynamic properties, notably the Gibbs Free
282   Energy.

283   In the current contribution, Langmuir model was used as the starting point to set the stage
284   for the forthcoming discussions on thermodynamic approaches and models that can be
285   established from ITC data analysis. However, shortcomings of the Langmuir model were rapidly
286   debatable by considering the circular dichroism and light scattering results. The Hill equation
287   was tested as an alternative thermodynamic equilibrium model in order to statistically improve
288   data fitting and the physico-chemical meaning of the fitting parameters were critically evaluated.

289   Circular dichroism results showed that lysozyme changes its native conformation upon
290   adsorption on the silica surface (Figure 3). One of the expected outcome of the observed
291   conformational changes is the spreading of the protein [57] which complicates the comparison
292   between the experimental coverage and the theoretically calculated mono-layer with the
293   Langmuir and Hill models. Furthermore, light scattering results showed that silica flocculates
294   due to protein bridging which complicates the estimation of the fractional surface area
295   occupancy due to the unknown stoichiometry of protein bridging. In other words, assuming the
296   mole fraction of bridging protein as m, unless the stoichiometry of the complex "*silica-*
297   *(lysozyme)$_m$-silica*" is resolved, fractional surface occupancy could not be predicted exactly.

298   As shown in the Figure 1, fitting the data with Langmuir equation does not yield a very
299   representative model describing the experimental findings. Nevertheless fitted maximum surface
300   coverage (1.5 mg/m^2) is between the experimental saturation (1.3 mg/m^2) and calculated
301   theoretical value based on monolayer coverage (1.7 mg/m^2, see the ESI for more details).
302   Comparing the experimental surface coverage and the theoretical monolayer coverage, the extent
303   of the adsorption of lysozyme on silica could be explained by at least three "possible" scenarios:
304   1) Projected cross sectional area of an unfolded protein might be slightly larger than that of the
305   folded native one. If this were the case, the silica surface would be covered with less protein.
306   That would support the slight discrepancy between the fittings and the observations. 2) At least
307   two silica particles are bridged by the same single protein through two binding sites. If this were
308   the case, available surface for adsorption would be dynamically decreasing and the saturation
309   would occur at a lower protein loading than the predicted. 3) Centrifugal forces applied to
310   separate the free protein during the non-direct adsorption technique, may detach some of the

311 bound protein on the silica as well. If this were the case, detached proteins would be assumed to
312 be weakly bound compared to the ones resisting centrifugal forces.

313   From a mathematical point of view, the Langmuir equation could be stretched to the Hill
314 equation by including an exponential term (n_{hill}). Increasing steepness in the isotherm yields n_{hill}
315 values larger than 1 and decreasing steepness yields n_{hill} values smaller than 1. As shown in
316 Figure 1, incorporating the exponential term (n_{hill}=1.7) improves the fitting (surface coverage
317 =1.3 mg/m^2). The improvement in the fitting justifies a further discussion on the physico-
318 chemical interpretation of the proposed stretching.

319   It has been stated that the exponential term in the Hill equation accounts for cooperativity
320 with $n_{hill} > 1$ indicating positive-cooperativity whereas $n_{hill} < 1$ indicates negative cooperativity
321 [58]. It is important to mention that cooperativity might reflect different situations depending on
322 the nature of the macromolecular interactions. For instance, in the case of protein adsorption,
323 formation of dimers on the sorbent surface or multiple interactions of proteins with the sorbent
324 are examples of such interactions [59]. So the initial steepness of the isotherm could be interpreted
325 as a positive cooperativity brought by the additional molecular interactions on the sorbent
326 surface. As indicated in Figure 1, even though experimental restrictions limited the resolution of
327 the adsorption isotherm at low equilibrium concentrations, the association of proteins was
328 expected to steepen the adsorption isotherm, which is referred as "positive cooperativity" [60].

329   The most plausible explanation of the positive cooperativity observed in the current study
330 is either the favorable lysozyme-lysozyme interactions on the silica surface [61] or multiple
331 contacts of lysozyme with silica particles [62]. More specifically, conformational changes could
332 be promoting the unfolded lysozyme to interact with the folded (native)/unfolded lysozyme [63]
333 or multiple binding sites on the lysozyme might allow multiple interactions with silica particles
334 [64].

335   Equilibrium constants that are predicted via Langmuir or Hill models are further
336 compared with the ones obtained from ITC experiments detailed in the following section.

337   **ITC provides more details on the mechanism of protein adsorption and resulting**

338   **bridging flocculation**

339   The most important objective of the current contribution was to investigate the
340 thermodynamics nature of the complex formation between silica nanoparticles and lysozyme in
341 which the protein adsorption plays a key role by inducing bridging flocculation. In this context,
342 the thermodynamics of the complex formation was further investigated by directly measuring the
343 heat of interactions through isothermal titration calorimetry (ITC) and the thermodynamic
344 parameters are reported as "apparent" parameters due to the simultaneous occurring multiple
345 binding events such as adsorption and flocculation.

346   The most remarkable outcome of the ITC results was the consistent (see the ITC master
347   curve in ESI, Figure 3) bimodal characteristic of the heat profile (Figure 4B) that cannot be
348   simply attributed to only one type of lysozyme-silica interaction. Results show that there were
349   two distinct heats (or enthalpies in this case due to constant pressure and volume conditions in
350   the ITC experiments) associated with two different modes of interactions leading to
351   complexation.

352   Further analysis of the thermodynamic signature associated with the complexation
353   process requires assuming a binding model for complexation and obtaining the equilibrium
354   constant from the known total concentrations of lysozyme and silica since the enthalpy of
355   binding is proportional to the change in the concentration of the bound lysozyme through each
356   injection. By using two sets of independent binding sites model, it was possible to discriminate
357   the free energy of the interactions into its enthalpy and entropy components by using apparent
358   association/dissociation constants. Even though the measured heat is the cumulative heat of all
359   simultaneous binding interactions including the silica flocculation that is promoted by lysozyme
360   bridging, it would not be unreasonable to propose that lysozyme binds to silica at least by two
361   distinct modes.

362   Initially, silica surface is strongly negatively charged with a hydrophilic character. The
363   higher affinity binding mode that is observed at lower molar ratios seems to correspond to
364   "bridging" interactions of lysozyme with silica at low surface coverage's that leads to the most
365   important portion of silica flocculation (see the initial jump in figure 2B). Higher calculated
366   positive entropy changes supports the assumption of significant disruption of the structurally
367   organized water at the silica surface which is the only possibility of overcoming silica's unusual
368   stability.

369   The stronger interactions at lower molar ratios could be arising from simultaneous
370   multiple interactions of lysozyme with silica particles or with lysozyme molecules. More
371   specifically, at low molar ratios, the same single protein might be binding to two silica particles
372   with two binding sites that are at opposite ends of the protein. This hypothesis would not conflict
373   with molecular dynamic simulation studies that showed evidence of two-charged surface
374   adsorption sites on lysozyme, the major one being at the N,C-terminal and the minor one being at
375   the Arg68 which is located almost opposite to the N, C-terminal phase [64] . Another possible
376   explanation to stronger interactions at lower molar ratios could be the favorable unfolded
377   protein-unfolded/folded protein interactions. In fact, partially unfolded lysozyme might have an
378   increased structural heterogeneity that promotes association among unfolded/folded lysozyme
379   [65].

380   As the complexation proceeds to higher molar ratios, the surface characteristics of the
381   "binding substrate" change accordingly. At molar ratio close to 20, the net charge of the complex
382   is zero which means that the number of positive and negative charges is the same. In fact this is
383   the molar ratio at which the first binding mode reaches to an equilibrium. After the first

384 equilibrium, the second binding mode takes over. The transition between binding modes could
385 be attributed to simultaneous neutralization and charge reversal events. Referring back to the
386 proposed multiple binding sites of lysozyme, it seems like until the zeta potential is zero, both
387 binding sites are involved in the electrostatic interactions with silica. After this point, while the
388 major binding site interacts with the remaining negative charge, minor binding sites provide the
389 silica surface with positive charges mainly due to a decreased number of silica particles available
390 for bridging. In fact, even after lysozyme completely dominates the surface charge distribution
391 (at a molar ratio of 50) the reaction still remains exothermic. Preserved exothermic nature of the
392 ITC signal at mole ratios that are close to saturation could be a sign of protein-protein
393 interactions which could be explained by the further formation of non-covalent bonds (protein
394 aggregation) [66].

395 Thus, the lower affinity binding mode observed at higher surface coverages/high molar
396 ratios seems to be resulting from limited protein-silica interactions combined with protein-
397 protein interactions. A lower positive entropy change supports the less significant effect of the
398 water/ion reorganization on the silica surface or at the binding interface. The reduced protein
399 silica interactions might be resulting from the fact that there is not enough available silica to bind
400 the second binding site of the lysozyme, and protein-protein interactions (protein aggregation)
401 might be resulting from formation of favorable hydrogen bonds [67].

402 In the present study, release of bound water to the bulk or reorganization to a more
403 disordered state at the silica-lysozyme interface is the possible reason behind the observed
404 favorable entropic contribution that compensates the unfavorable entropic contribution created
405 by the movement restriction of the protein between silica particles. Similar to the disruption of
406 the hydration shell, counter ion release from charged surfaces to bulk and charge regularization
407 upon complexation are also expected to contribute to the estimated entropy gain. Indeed the
408 effect of counter ions have been highlighted in recent studies where proteins bind on
409 polyelectrolyte brushes on the wrong side of interactions. Bearing in mind that silica is stable
410 against aggregation even at the isoelectric point, disruption of hydration shell is proposed to be
411 the main source of entropy gain as it was in Rotello's studies [16]. Last but not least, it is
412 important to remember that the partial transition in the secondary structure of the protein (from
413 helix to sheets and random coil (Figure 3B) supports the hypothesis that the protein conformation
414 change might be contributing to the estimated favorable entropy change.

415 Even though the electrostatic interactions are not quantitatively dominating the complex
416 formation, it is believed that incorporating them at an intermediate level makes it possible to
417 estimate the contribution of entropy from the curve fitting analysis. Increasing the salt
418 concentration could have helped to better resolve the proposed protein–protein interactions,
419 however screening the charges would make the complexation even more entropic and it would
420 be problematic or even impossible to measure these interactions with the current sensitivity of
421 the ITC systems used in this study [50].

422   It is already mentioned that, since complexation includes both protein adsorption and
423   silica flocculation, the equilibrium constants and the free energy and entropy obtained from these
424   values can be considered as apparent parameters and absolute numbers should be evaluated
425   carefully. (Due to the extraordinary stability of colloidal silica against aggregation, it is not
426   possible to test silica aggregation using ITC and subtract this from the complexation to find the
427   heat related to the interactions of silica with lysozyme, or namely adsorption). However, it is
428   quite interesting to observe that the high affinity binding dissociation constant has almost the
429   same order of magnitude as the one obtained from Hill equation (3.15×10^{-8}) and the low affinity
430   binding dissociation constant has the same order of magnitude as the one obtained from the
431   Langmuir model (2.65×10^{-6}). This gives confidence to assume a binding mechanism (multiple
432   binding site model) and resolve the affinity of the lysozyme binding on hydrophilic nano-silica.

433   **<u>Conclusions</u>**

434   Thermodynamics of protein-nanoparticle interactions and complexation were studied
435   with a well-defined model system (lysozyme-silica). Interactions governing protein nanoparticle
436   complexation appears to be complex yet resolvable with a multi-experimental approach.
437   Electrostatically initiated protein adsorption plays the key-role in complexation by inducing
438   bridging flocculation. Examination of complexation by ITC showed a bimodal character due to
439   two distinct binding modes, a higher affinity binding mode that is driven by a larger entropic
440   contribution followed by a low affinity binding mode that is a consequence of moderate enthalpy
441   and entropic contributions. The higher affinity mode requires less protein to reach equilibrium
442   and is observed at lower surface coverages. Solvent re-organization plays an important role in
443   the complexation process by contributing to a favorable entropy gain. In addition to solvent
444   reorganization, changes in the secondary structure of lysozyme upon adsorption and counter ion
445   release might be contributing to the favorable entropy gain. The dominant entropic pathway of
446   complexation showed that the assembly of the supra colloidal micro-structures by using
447   nanoparticles and biopolymers as building blocks might not be limited by unfavorable enthalpic
448   restrictions. Dominant entropic pathway of nano-bio complexation might open up the possibility
449   for many other specific applications by using nano-bio hybrid designs.

450   **<u>Acknowledgment</u>**

459   The authors declare that they have no competing interests.

460   **Figure 1** Adsorption isotherms: Squares and brackets represent mean and standard error of the
461   mean (n=6, triplicate short equilibrium times, triplicate 16 hours equilibrium), respectively. Blue
462   and red lines indicate the fittings of adsorption isotherms via Langmuir and Hill models,
463   respectively. The gray background in the figure is the detection limit of the BCA assay so the
464   first two data points remarked with an asterisk should be interpreted with caution.

465   **Figure 2** Light Scattering results. 2A. Zeta Potential of lysozyme-silica complexes. Charge of
466   silica particles before any protein incorporation (Mole Ratio=0) is marked with a blue arrow.
467   Second y-axis (red) represents the charge scale for lysozyme. 2B. Hydrodynamic radius of
468   lysozyme-silica complex. Radius of silica particles before any protein incorporation (Mole
469   Ratio=0) is marked with a blue arrow. (The lines on the data points are drawn as a guide to the
470   eye)

471   **Figure 3** Circular Dichroism. (A) CD spectra of control and bound proteins. MRE stands for
472   mean residue ellipticity and MR for molar ratio. (B). Deconvolution of CD spectra that enable
473   the determination of different types of secondary structure; helix, sheet and turn. (The lines on
474   the data points are drawn as a guide to the eye)

475   **Figure 4** ITC results. (A) ITC raw data before integration: After the "first load", the syringe was
476   re-filled with the same protein solution and injected to the cell that contained silica and lysozyme
477   to collect the "second load" heat. (B) Integrated peaks after normalization as a function of Mole
478   Ratio. After integrating the peaks of raw data with respect to time, the obtained heats were
479   normalized with respect to initial protein molarity. Red line represents the heat profile fitted with
480   the multiple site model.

481   **Figure 5**. ITC thermodynamics signature. ΔH is measured directly with ITC, ΔG and ΔS were
482   calculated based on the equilibrium constant as explained in the text. T is the test temperature,
483   which is 298.15K in this case.

484   **Table 1** ITC Apparent binding parameters obtained from the ITC experiments and the multiple
485   site model. K_a is the equilibrium association constant, K_d is the equilibrium disassociation
486   constant, n is the stoichiometry, ΔH is the enthalpy change, ΔS is the entropy change and ΔG is
487   the Gibbs free energy change.

ITC Parameter	*Site 1*	*Site 2*
K_a **(M^{-1})**	4.65E+08	3.2E+05
K_d **(M)**	2.15E-09	8.40E-06
n	7.549	54.72
ΔH (kJ/mol)	-14.84	-12.16
ΔS (J/mol.K)	122	56.4
ΔG (kJ/mol)	-51.15	-28.96

488

489

490

491   <u>**References**</u>

492   1. Lynch, I., and Dawson, K. A. (2008) Protein-nanoparticle interactions, *Nano Today 3*,
493   40-47.
494   2. Nel, A. E., Madler, L., Velegol, D., Xia, T., Hoek, E. M. V., Somasundaran, P.,
495   Klaessig, F., Castranova, V., and Thompson, M. (2009) Understanding biophysicochemical
496   interactions at the nano-bio interface, *Nature Materials 8*, 543-557.
497   3. Leszczynski, J. (2010) Bionanoscience: Nano meets bio at the interface, *Nature Nano*
498   *5*, 633-634.
499   4. Moyano, D. F., and Rotello, V. M. (2011) Nano meets biology: Structure and function
500   at the nanoparticle interface, *Langmuir 27*, 10376-10385.
501   5. Niemeyer, C. M. (2001) Nanoparticles, proteins, and nucleic acids: Biotechnology
502   meets materials science, *Angewandte Chemie International Edition 40*, 4128-4158.
503   6. You, C.-C., Verma, A., and Rotello, V. M. (2006) Engineering the nanoparticle-
504   biomacromolecule interface, *Soft Matter 2,* 190-204.
505   7. Cedervall, T., Lynch, I., Lindman, S., Berggård, T., Thulin, E., Nilsson, H., Dawson,
506   K. A., and Linse, S. (2007) Understanding the nanoparticle–protein corona using methods to
507   quantify exchange rates and affinities of proteins for nanoparticles, *Proceedings of the National*
508   *Academy of Sciences 104*, 2050-2055.
509   8. Lynch, I., Cedervall, T., Lundqvist, M., Cabaleiro-Lago, C., Linse, S., and Dawson, K.
510   A. (2007) The nanoparticle-protein complex as a biological entity; a complex fluids and surface
511   science challenge for the 21st century, *Advances in Colloid and Interface Science 134-135*, 167-
512   174.
513   9. Lynch, I., Salvati, A., and Dawson, K. A. (2009) Protein-nanoparticle interactions:
514   What does the cell see?, *Nat Nano 4,* 546-547.
515   10. Katz, E., and Willner, I. (2004) Integrated nanoparticle–biomolecule hybrid systems:
516   Synthesis, properties, and applications, *Angewandte Chemie International Edition 43,* 6042-
517   6108.
518   11. Asuri, P., Bale, S. S., Karajanagi, S. S., and Kane, R. S. (2006) The protein–
519   nanomaterial interface, Current Opinion in Biotechnology 17, 562-568.
520   12. Kane, R. S., and Stroock, A. D. (2007) *Nanobiotechnology: Protein-nanomaterial*
521   *interactions, Biotechnology Progress* 23, 316-319.
522   13. Li, F., Josephson, D. P., and Stein, A. (2011) Colloidal assembly: The road from
523   particles to colloidal molecules and crystals, *Angewandte Chemie International Edition 50*, 360-
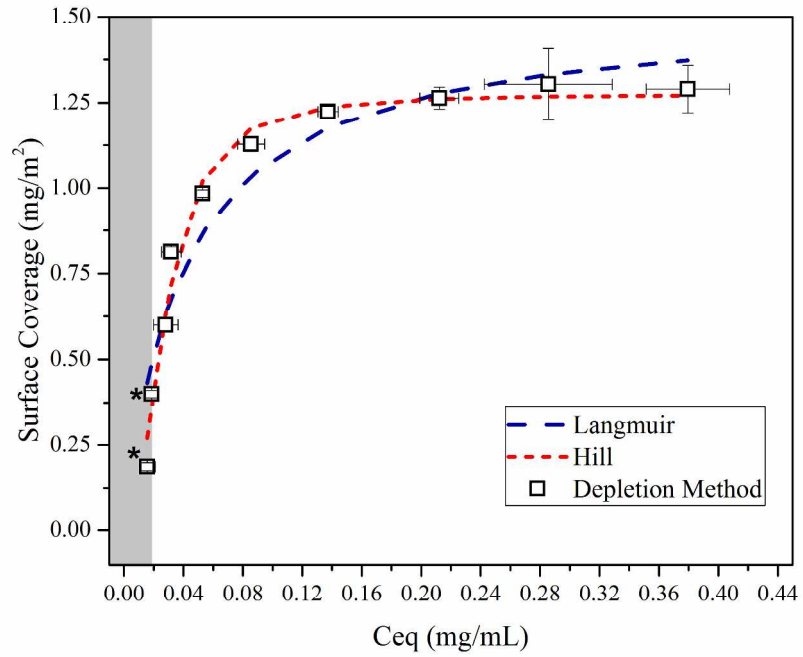524   388.
525   14. Velev, O. D., and Gupta, S. (2009) Materials Fabricated by Micro- and Nanoparticle
526   Assembly – The Challenging Path from Science to Engineering, *Advanced Materials 21*, 1897-
527   1905.

15. Costanzo, P. J., Patten, T. E., and Seery, T. A. P. (2004) Protein−ligand mediated aggregation of nanoparticles: A study of synthesis and assembly mechanism, *Chemistry of Materials 16,* 1775-1785.

16. De, M., Miranda, O. R., Rana, S., and Rotello, V. M. (2009) Size and geometry dependent protein-nanoparticle self-assembly, *Chemical Communications*, 2157-2159.

17. Salem, A. K., Chen, M., Hayden, J., Leong, K. W., and Searson, P. C. (2004) Directed Assembly of Multisegment Au/Pt/Au Nanowires, Nano Letters 4, 1163-1165.

18. Huang, R., Carney, R.P., Stellacci, F., and B.L.T. Lau, B.L.T. (2013) Protein–nanoparticle interactions: the effects of surface compositional and structural heterogeneity are scale dependent, *Nanoscale, 5,* 6928-6935.

19. Bayraktar, H., Srivastava, S., You, C.-C., Rotello, V. M., and Knapp, M. J. (2008) Controlled nanoparticle assembly through protein conformational changes, *Soft Matter 4*, 751-756.

20. Bharti, B., Meissner, J., and Findenegg, G. H. (2011) Aggregation of silica nanoparticles directed by adsorption of lysozyme*, Langmuir 27 (16),* 9832-9833.

21. Moerz, S.T., Kraegeloh, A., Chanana, M., and Kraus, T. (2015) Formation mechanism for stable hybrid clusters of proteins and nanoparticles *, ACS Nano 9*, 6696-6705.

22. Eren, N., Jones, O., and Campanella, O. (2015) Changes in the rheology of nano-structured suspensions by adsorption of the protein α-lactalbumin on the surface of silica particles, *Rheologica Acta 54*, 735-744.

23. Bergna, H. E., and Roberts, W. O. (2005) Colloidal silica: Fundamentals and applications, *CRC Press*.

24. Blake, C. C., Koenig, D. F., Mair, G. A., North, A. C., Phillips, D. C., and Sarma, V. R. (1965) Structure of hen egg-white lysozyme: A three-dimensional Fourier synthesis at 2 Angstrom resolution, *Nature 206*, 757-761.

25. Deželić, G., and Kratohvil, J. P. (1960) Determination of size of small particles by light scattering. Experiments on ludox colloidal silica, *Kolloid-Zeitschrift 173*, 38-48.

26. Daly, S. M., Przybycien, T. M., and Tilton, R. D. (2003) Coverage-dependent orientation of lysozyme adsorbed on silica, *Langmuir 19*, 3848-3857.

27. Hildebrand, N., Köppen, S., Derr, L., Li, K., Koleini, M., Rezwan, K., and Colombi Ciacchi, L. (2015) adsorption orientation and binding motifs of lysozyme and chymotrypsin on amorphous silica, *The Journal of Physical Chemistry C* 119, 7295-7307.

28. Rezwan, K., Meier, L. P., and Gauckler, L. J. (2005) Lysozyme and bovine serum albumin adsorption on uncoated silica and AlOOH-coated silica particles: The influence of positively and negatively charged oxide surface coatings, *Biomaterials 26*, 4351-4357.

29. Xu, K., Ouberai, M. M., and Welland, M. E. (2013) A comprehensive study of lysozyme adsorption using dual polarization interferometry and quartz crystal microbalance with dissipation*, Biomaterials 34*, 1461-1470.

30. Norde, W., and Favier, J. P. (1992) Structure of adsorbed and desorbed proteins, *Colloids and Surfaces 64*, 87-93.
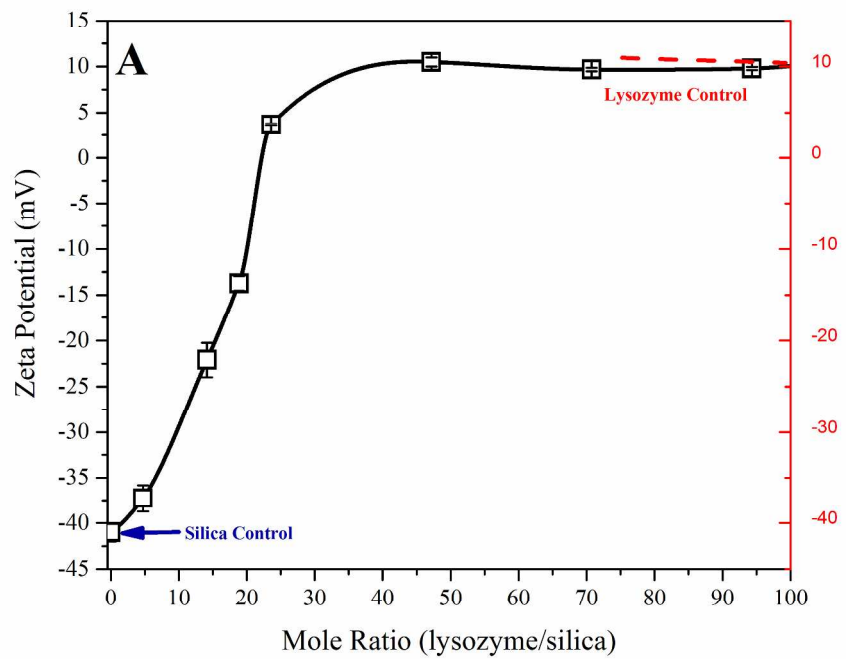
568   31. Koppel, D. E. (1972) Analysis of macromolecular polydispersity in intensity
569   correlation spectroscopy: The method of cumulants, *The Journal of Chemical Physics 57*, 4814-
570   4820.

571   32. Reference Manual, M. I. (2007) Sample Dispersion and Refractive Index Guide.

572   33. Zhang, L., Song, J., Newhouse, Y., Zhang, S., Weisgraber, K. H., and Ren, G. (2010)
573   An optimized negative-staining protocol of electron microscopy for apoE4•POPC lipoprotein,
574   *Journal of Lipid Research 51,* 1228-1236.

575   34. Greenfield, N. J. (2006) Using circular dichroism spectra to estimate protein
576   secondary structure, *Nature Protocols 1,* 2876-2890.

577   35. Sreerama, N., and Woody, R. W. (2000) Estimation of protein secondary structure
578   from circular dichroism spectra: Comparison of CONTIN, SELCON, and CDSSTR methods
579   with an expanded reference set, *Analytical Biochemistry 287*, 252-260.

580   36. Whitmore, L., and Wallace, B. A. (2008) Protein secondary structure analyses from
581   circular dichroism spectroscopy: Methods and reference databases, Biopolymers 89, 392-400.

582   37. Velazquez-Campoy, A., and Freire, E. (2006) Isothermal titration calorimetry to
583   determine association constants for high-affinity ligands, *Nat. Protocols 1,* 186-191.

584   38. Freire, E., Mayorga, O. L., and Straume, M. (1990) Isothermal titration calorimetry,
585   *Analytical Chemistry 62,* 950A-959A.

586   39. Haynes, C. A., and Norde, W. (1994) Globular proteins at solid/liquid interfaces,
587   *Colloids and Surfaces B: Biointerfaces 2,* 517-566.

588   40. Turci, F., Ghibaudi, E., Colonna, M., Boscolo, B., Fenoglio, I., and Fubini, B. (2010)
589   An integrated approach to the study of the interaction between proteins and nanoparticles,
590   *Langmuir 26*, 8336-8346.

591   41. Kumar, S., Aswal, V. K., and Callow, P. (2014) pH-Dependent interaction and
592   resultant structures of silica nanoparticles and lysozyme protein, *Langmuir 30,* 1588-1598.

593   42. Felsovalyi, F., Mangiagalli, P., Bureau, C., Kumar, S. K., and Banta, S. (2011)
594   Reversibility of the adsorption of lysozyme on silica, *Langmuir 27,* 11873-11882.

595   43. Czeslik, C., and Winter, R. (2001) Effect of temperature on the conformation of
596   lysozyme adsorbed to silica particles, *Physical Chemistry Chemical Physics 3*, 235-239.

597   44. Sethuraman, A., Vedantham, G., Imoto, T., Przybycien, T., and Belfort, G. (2004)
598   Protein unfolding at interfaces: Slow dynamics of α-helix to β-sheet transition, *Proteins:
599   Structure, Function, and Bioinformatics* 56, 669-678.

600   45. Vertegel, A. A., Siegel, R. W., and Dordick, J. S. (2004) Silica nanoparticle size
601   influences the structure and enzymatic activity of adsorbed lysozyme, Langmuir 20, 6800-6807.

602   46. Wu, X., and Narsimhan, G. (2008) Effect of surface concentration on secondary and
603   tertiary conformational changes of lysozyme adsorbed on silica nanoparticles, *Biochimica et
604   Biophysica Acta (BBA) - Proteins and Proteomics 1784,* 1694-1701.

605   47. Kabsch, W., and Sander, C. (1983) Dictionary of protein secondary structure -
606   pattern-recognition of hydrogen-bonded and geometrical features, *Biopolymers 22*, 2577-2637.

48. Vedantham, G., Sparks, H.G., Sane, S.U. and Tzannis, S., and Przybycien, T.M. (2000) A holistic approach for protein secondary structure estimation from infrared spectra in h$_2$o solutions, *Analytical Biochemistry 285,* 33-49

49. Boczkowska, M., Rebowski, G., Kast, D. J., and Dominguez, R. (2014) Structural analysis of the transitional state of Arp2/3 complex activation by two actin-bound WCAs, *Nat Commun ,* 1-12.

50. De, M., You, C.-C., Srivastava, S., and Rotello, V. M. (2007) Biomimetic interactions of proteins with functionalized nanoparticles: A thermodynamic study, *Journal of the American Chemical Society 129*, 10747-10753.

51. Witteman, A., and Ballauff, M. (2006) Interaction of proteins with linear polyelectrolytes and spherical polyelectrolyte brushes in aqueous solution, *Physical Chemistry Chemical Physics 8*, 5269-5275.

52. Henzler, K., Haupt, B., Lauterbach, K., Witteman, A., Borisov, O., and Ballauff, M. (2010) Adsorption of B-lactoglobulin on spherical polyelectrolyte brushes: Direct proof of counter ion release, *Journal of the Americal Chemical Society 132*, 3159-3163.

53. Harries, D., May, S., and Ben-Shaul, A. (2013) Counterion release in membrane - biopolymer interactions, Soft Matter 9, 9268-9284.

54. Nakanishi, K., Sakiyama, T., and Imamura, K. (2001) On the adsorption of proteins on solid surfaces, a common but very complicated phenomenon, *Journal of Bioscience and Bioengineering 91*, 233-244.

55. Rabe, M., Verdes, D., and Seeger, S. (2011) Understanding protein adsorption phenomena at solid surfaces, *Advances in Colloid and Interface Science 162*, 87-106.

56. McGuire, J. (2014) Building a working understanding of protein adsorption with model systems and serendipity, *Colloids and Surfaces B: Biointerfaces 124*, 38-48.

57. Van der Veen, M., Stuart, M.C., Norde, W. (2007) Spreading of proteins and its effect on protein and desorption kinetics*, Colloids and Surfaces B: Biointerfaces* 54, 136-142.

58. Foo, K.Y., and Hameed, B.H. (2010) Insights into modelling of adsorption isotherm systems, *Chemical Engineering Journal 116*, 2-10.

59. Luo, Q., and Andrade, J.D. (1998) Cooperative adsorption of proteins onto hydroxyapatite, *Journal of Colloid and interface Science 200,* 104-113.

60. Chatelier, R.C., and Minton A.P. (1996) Adsorption of globular proteins on locally planar surfaces: models for the effect of excluded surface area and aggregation of adsorbed protein on adsorption equilibria, *Biophysical Journal 71*, 2367-2374.

61. Ball, V., and Ramsden J.J. (2000) Analysis of hen egg white lysozyme adsorption on Si(Ti)O$_2$ | aqueous solution interfaces at low ionic strength: a biphasic reaction related to solution self-association, *Colloids and Surfaces B: Biointerfaces 17,* 81–94.

62. Dismer, F., Petzold, M., Hubbuch, J. (2008) Effects of ionic strength and mobile phase pH on the binding orientation of lysozyme on different ion-exchange adsorbents, *Journal of Chromatography A,* 1194, 11–21.
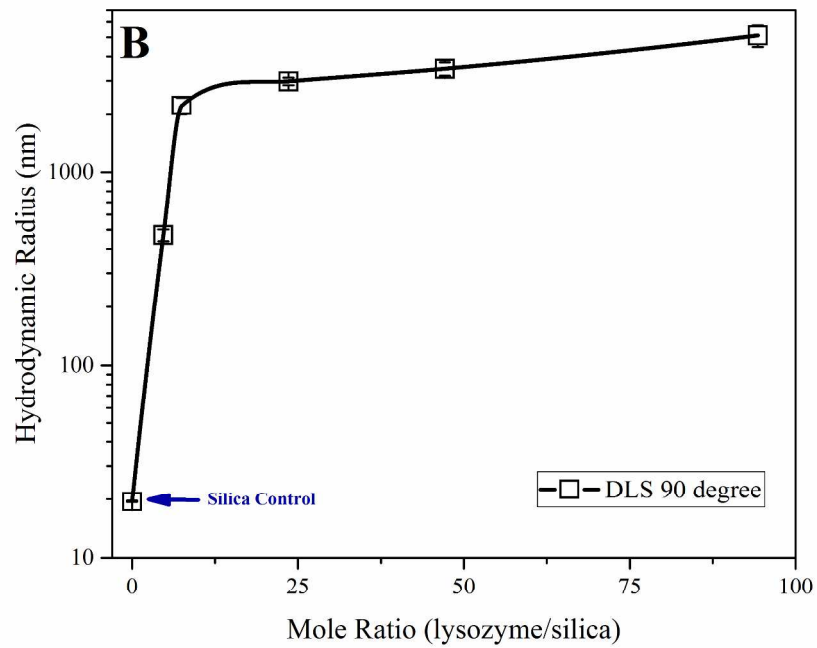
646   63. Sethuraman, A., and Belfort, G. (2005) Protein structural perturbation and
647   aggregation on homogeneous surfaces, *Biophysical Journal 88*, 1322–1333.

648   64. Kubiak-Ossowska, K., and Mulheran, P.A. (2010) Mechanism of hen egg white
649   lysozyme adsorption on a charged solid surface *Langmuir 26*, 15954–15965.

650   65. Larsericsdotter, H., Oscarsson, S., Buijs, J. (2004) Thermodynamic analysis of
651   lysozyme adsorbed to silica, *Journal of Colloid and Interface Science 276*, 261–268.

652   66. Ikenouea, T., Leea, Y.-H., Kardosb, J., Yagia, H., Ikegamia, T., Naikic, H., and
653   Gotoa, Y. (2014) Heat of supersaturation-limited amyloid burst directly monitored by isothermal
654   titration calorimetry, *Proceedings of the National Academy of Sciences 111*, 6654-6659.

655   67. O'Brien, R., and Haq, I. (2004). Applications of biocalorimetry: binding, stability and
656   enzyme kinetics. In: *Biocalorimetry 2: Applications of calorimetry in the biological sciences*,
657   Ladbury, J.E., and Doyle, M.L. John Wiley& Sons Ltd., Chichester, U.K. pp 3-34.
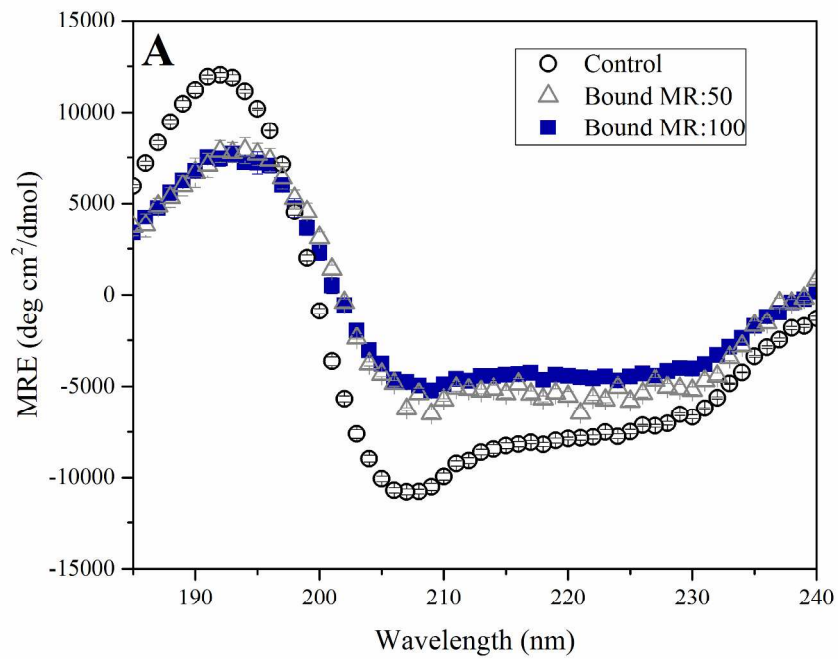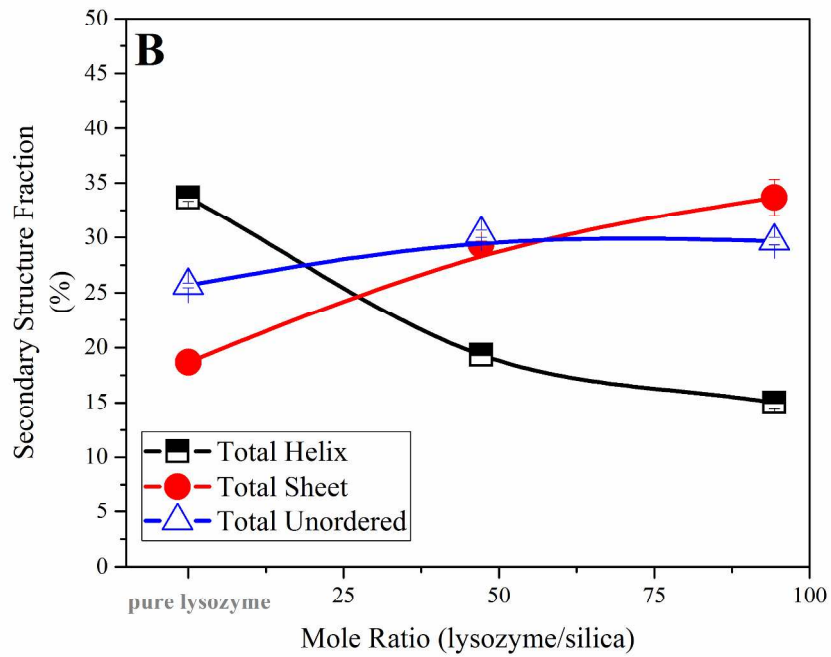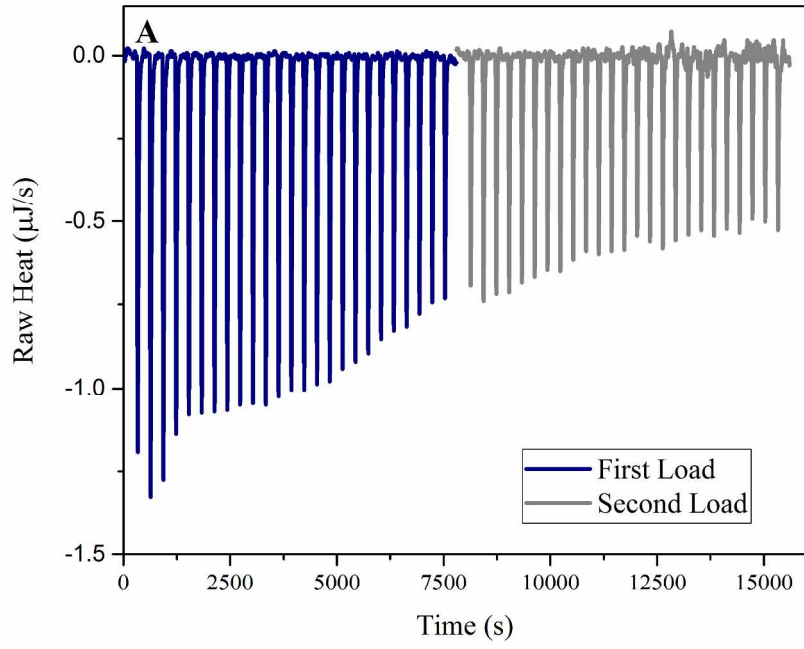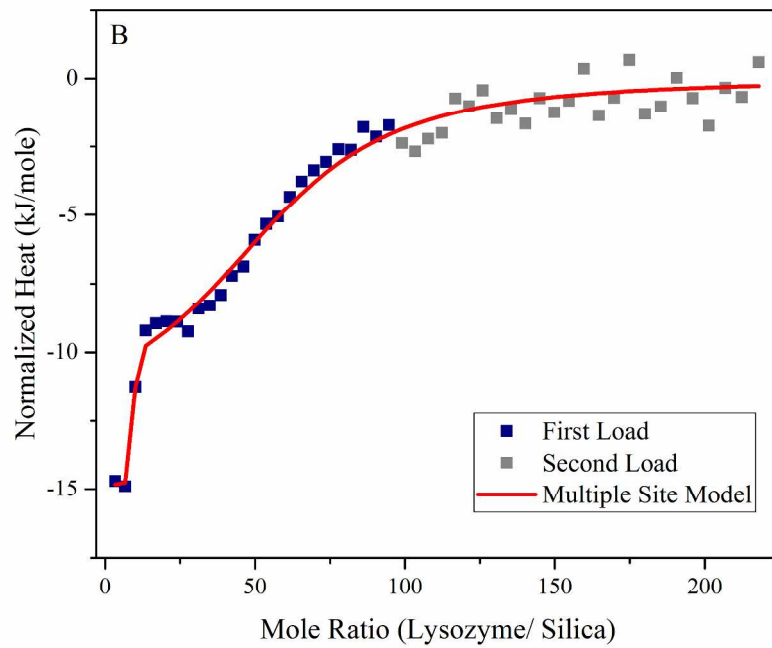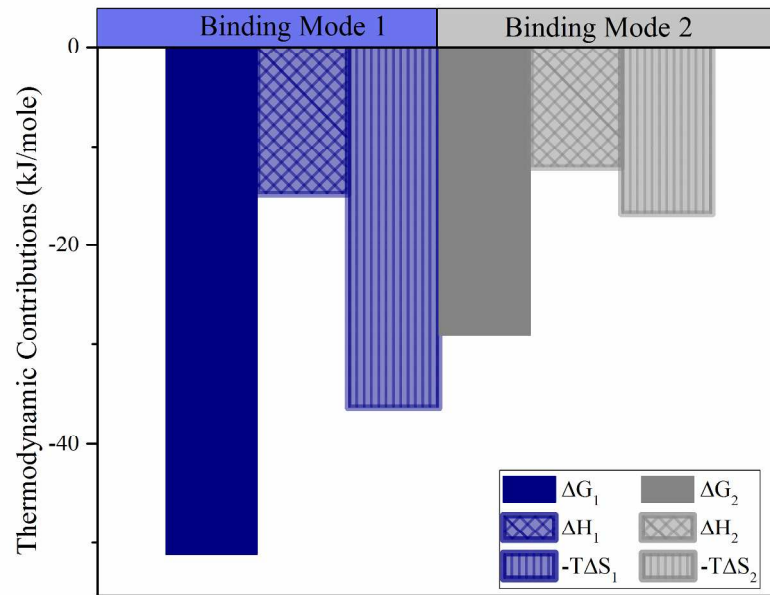
658

272x208mm (300 x 300 DPI)

272x208mm (300 x 300 DPI)

272x208mm (300 x 300 DPI)

272x208mm (300 x 300 DPI)

272x208mm (300 x 300 DPI)

272x208mm (300 x 300 DPI)

272x208mm (300 x 300 DPI)

272x208mm (300 x 300 DPI)